Nonlinear Processes in Geophysics (1999) 6: 221–228

Nonlinear Processes in Geophysics

Theory of localized bipolar wave-structures and nonthermal particle distributions in the auroral ionosphere

M. V. Goldman[1], M. M. Oppenheim[2], and D. L. Newman[1]

[1]Center for Integrated Plasma Studies, University of Colorado, Boulder, CO 80309-0390, USA
[2]Astronomy Department, Boston University, Boston, MA 02215, USA

Received: 22 June 1999 – Revised: 3 September 1999 – Accepted: 7 September 1999

Abstract. Bipolar wave structures and nonthermal particle distributions measured by the FAST satellite in regions of downward current are interpreted in terms of the nonlinear evolution of a two-stream instability. The instability results in holes, both in the electron distribution in phase space and in the electron density in real space. The wave potential energy, which traps the electrons, has a single minimum, and the associated electric field is bipolar. The early bipolar structures are coherent over hundreds of Debye lengths in the direction perpendicular to the magnetic field. After thousands of plasma periods the perpendicular coherence is lost, the structures break up, and electrostatic whistlers begin to dominate. Simulations and preliminary analysis of this breakup and emission process are presented.

1 Measurements

Among the most interesting nonlinear phenomena observed on board the FAST satellite are the measurements of bipolar waveforms and nonthermal particle distributions in the presence of downward currents at altitudes in the auroral ionosphere between 2000 and 4000 km. Figure 1 shows measurements in a time interval exhibiting bipolar structures in the component of the wave electric field parallel to the geomagnetic field (Ergun et al., 1998). For the data set studied, the size of a bipolar structure, which we define as the distance between the parallel and antiparallel wave field extrema, was found to range from a few Debye lengths for the less intense events ($e\phi/T_e \ll 1$), to eight Debye lengths for the more intense events ($e\phi/T_e \sim O(1)$). Here, ϕ is the wave potential, T_e is the parallel temperature of the measured (nonthermal) electron distribution function, and the Debye length is defined in terms of T_e. A typical Debye length is on the order of 100 meters. The bipolar waveforms are inferred to be moving parallel to B at a large fraction of the mean electron velocity drift.

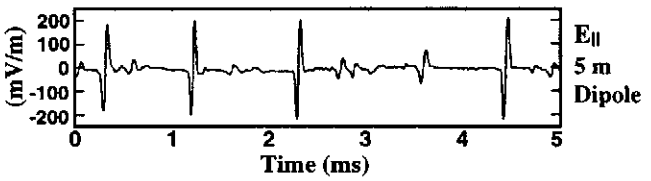

Fig. 1. Observed bipolar electric fields from Ergun et al. (1998).

The mean electron velocity is on the order of 2×10^6 m/s, which corresponds to tens of eV. This data set was selected according a number of criteria. One such criterion was that the perpendicular component of the waveform had to exhibit a unipolar structure. Bipolar events not contained in this data set were sometimes more intense (Carlson et al., 1998), less isolated, and less symmetric in the amplitude extrema of the parallel and antiparallel wave field of a given bipolar waveform. For these more intense measured events, the mean electron velocity drift can be as high as several keV, electric field peaks can be as high as one V/m, and potential drops as high as hundreds of volts. Coincident with the appearance of bipolar fields, magnetized waves are often detected at frequencies lying in the range of electrostatic whistlers, lower-hybrid, and ion-Bernstein waves.

Measurements of the particle distribution functions reveal them to be highly nonthermal, even at low velocities. A typical contour of constant phase-space density in the electron distribution function resembles the one shown in Figure 2. Thus, the parallel electron temperature is generally much larger than the perpendicular temperature. Distribution functions such as these are typically measured over relatively long time intervals containing many bipolar events. In contrast the ion distribution functions are often observed to be pancake-shaped, with perpendicular temperature much greater than the parallel temperature.

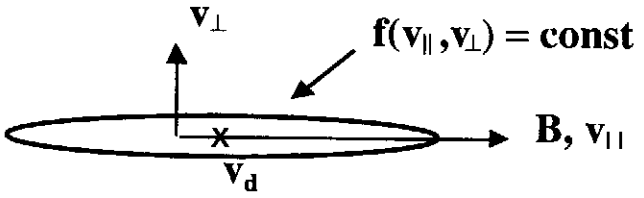

Fig. 2. Velocity-space contour of constant electron distribution has a "cigar" shape, with $T_\parallel \gg T_\perp$ and a mean velocity v_d.

2 Two-stream electron instability and 1-D evolution

The challenge to theory is to find an explanation for both the bipolar wave structures and the time-averaged distribution functions in terms of a minimal set of assumptions. We have shown (Goldman et al., 1998, 1999; Oppenheim et al., 1999) that the assumption of an initial two-stream instability is sufficient to explain many features of the measured wave structures and electron distribution functions. These include the wave structure polarity, spatial size, speed, and intensity, as well as the presence of low-frequency magnetized-plasma waves, and the field-alignment and nonthermal nature of the evolved electron velocity distribution.

The heuristic picture can be understood from long-known results of one-dimensional simulations of the evolution of the electron two-stream instability in a uniform and static ion background. A number of these features follow from the basic physics of the saturation of the two-stream instability, in which two cold counterstreaming electron beams with equal densities $n_e/2$ and velocities $\pm \mathbf{v}_b/2$ are unstable to a fastest-growing wave of wavenumber $k_* \propto \omega_e/v_b$. (The linear theory is addressed further in the next section.)

Early as well as recent one-dimensional kinetic simulations (Berk and Roberts, 1967; Morse and Nielson, 1969; Omura et al., 1996) of the nonlinear evolution of this instability show that saturation occurs when the potential energy $e\phi$ of the unstable wave grows large enough to trap a substantial fraction of beam electrons—leading to the formation of phase space "vortices" or "holes" (with no electrons in the lowest energy states), as shown in the phase-space distribution of Fig. 3. For such a hole, the wave potential energy is on the order of the "temperature" T_e of the *total* evolved electron distribution of the now-merged electron beams. Furthermore, both T_e and $e\phi$ are on the order of mv_b^2.

The potential ϕ supporting the phase-space hole is bell-shaped, so that its spatial derivative gives a bipolar-shaped wave electric field. In Fig. 4, spatial profiles are shown for a typical electron potential energy, $-e\phi(x)$, bipolar wave field, $-\partial_x\phi(x)$, and electron density (proportional to $\partial_x^2\phi + \text{const.}$ as a result of Poisson's equation).

In the frame of one of the beams, the phase-space hole and associated potential, bipolar structure, and density hole all move at $v_b/2$, which is the mean drift of the entire electron distribution.

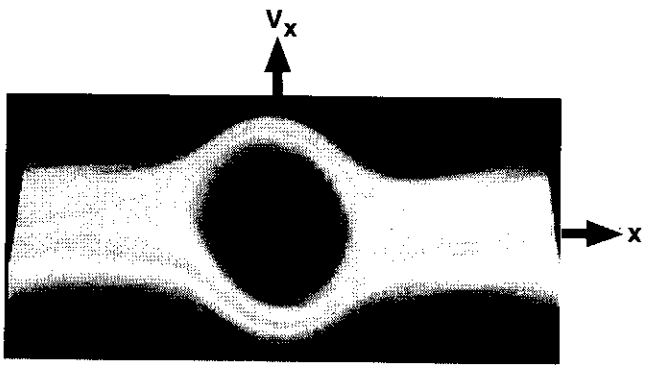

Fig. 3. Phase-space "vortex" hole from 1-D Vlasov simulation.

3 Linear theory of the two-stream instability in a 2-D plasma with strongly magnetized electrons

It is instructive to study the linear phase of the two-stream electron instability both with and without dynamic ions. Rather than restrict the analysis to one dimension, it is just as easy to study the cold fluid linear instability in two or three dimensions, provided we assume *infinitely magnetized electrons*. The condition for this approximation is that the electron cyclotron frequency Ω_e be much larger than both the electron plasma frequency ω_e and the wave frequency ω. The FAST observations of bipolar structures occur under just such conditions, since Ω_e/ω_e runs from 5 to 15 at relevant altitudes in the auroral ionosphere, and we are considering only waves with $\omega < \omega_e$. Working under these approximations in the symmetry frame where the two beams have equal and opposite velocities, it is easy to show that the dielectric function ϵ is

$$\epsilon = 1 - \frac{1}{2}\left[\frac{1}{(\Omega + K)^2} + \frac{1}{(\Omega - K)^2}\right], \qquad (1)$$

where $\Omega \equiv (\omega/\omega_e \cos\theta)$, $K \equiv kv_b/2\omega_e$, and θ is the angle between k and $\mathbf{B}$. The zeroes of ϵ determine the properties of the instability. The solutions to this biquadratic equation are $2\Omega^2 = (1+2K^2) \pm (1+8K^2)^{1/2}$. In Fig. 5, growth rates and frequencies are plotted. The purely growing mode (bold) peaks at about $\gamma = 0.4\omega_e \cos\theta$ and $K = 0.6$. In the limit of small K, the solutions are $\Omega^2 = 1$ and $\Omega^2 = -K^2$. These correspond to the following four solutions in this frame: $\Omega = \pm\omega_e \cos\theta$ and $\omega = \pm i(kv_b/2)\cos\theta$. The first two solutions are stable electrostatic whistlers (which are electron plasma waves when $k_y = 0$), while the second two consist of a purely growing unstable mode and a purely damped mode. In the "laboratory" frame, in which one of

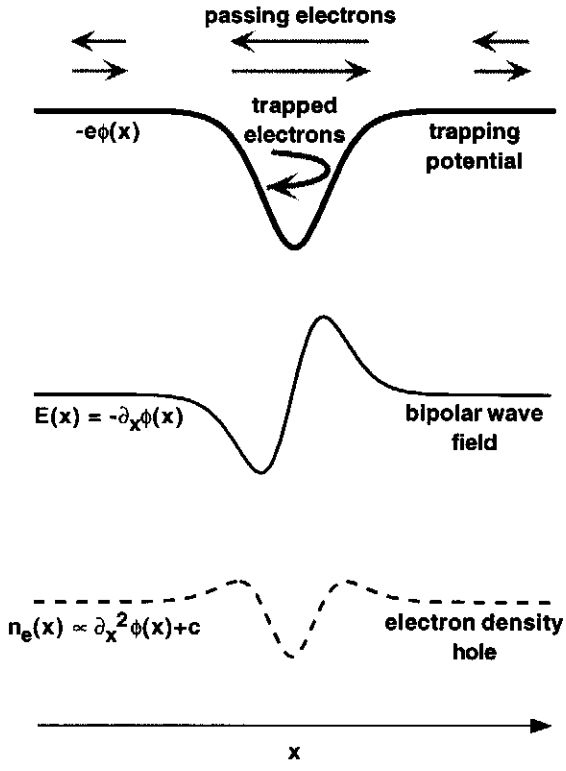

Fig. 4. Wave potential energy, bipolar field, and density hole as functions of x.

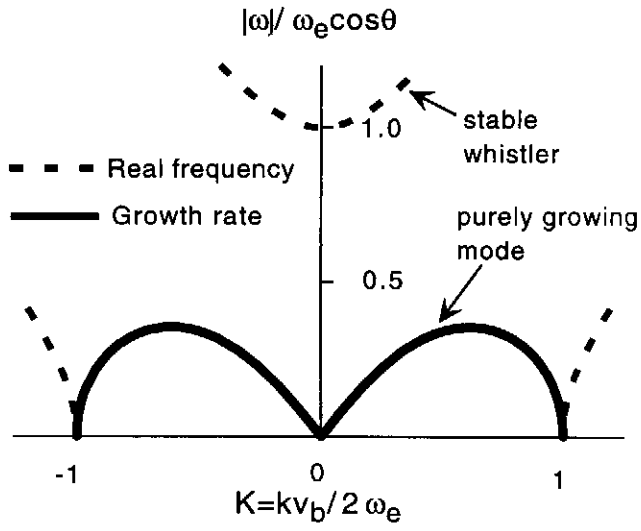

Fig. 5. Real and imaginary frequency solutions to $\epsilon = 0$ for $|\Omega| \equiv |\omega|/\omega_e \cos\theta$ as a function of $K \equiv kv_b/2\omega_e$.

the electron beams is stationary (so that the other is moving at v_b), all of these modes are Doppler shifted by $\delta\omega = (kv_b/2)\cos\theta$ and, in particular, the unstable purely growing mode becomes a kind of "beam" mode.

These results can be generalized to include ions. We solve the linearized fluid equations in the laboratory frame and add a component of cold *unmagnetized* stationary ions to the stationary cold *strongly magnetized* electrons. This is justified because in FAST measurements it is often the case that the electron cyclotron frequency is much larger than the electron plasma frequency ($\Omega_e \gg \omega_e$) while, at the same time, the ion cyclotron frequency is much smaller than the ion plasma frequency ($\Omega_i \ll \omega_i$). The ion density is equal to the sum of the densities of the two electron components. The dielectric function ϵ obtained from the cold fluid equations and Poisson's equation is now

$$\epsilon = 1 - \frac{\omega_i^2 + (\omega_e^2/2)\cos^2\theta}{\omega^2} - \frac{(\omega_e^2/2)\cos^2\theta}{(\omega - kv_b\cos\theta)^2} \qquad (2)$$

When there is no beam, the cold fluid dispersion relation reduces to $\omega^2 = \omega_i^2 + \omega_e^2\cos^2\theta$. This corresponds to an electrostatic whistler wave at frequency $\pm\omega_e\cos\theta$ connected to a lower hybrid wave at frequency ω_i in the limit $\theta \to \pi/2$. (The lower hybrid frequency reduces to the ion plasma frequency for strongly magnetized electrons and weakly magnetized ions.) The numerical solution for the zeroes of (2) will be shown later when comparing with PIC simulation results. Once again, there will be unstable "beam" modes (Doppler-shifted purely growing modes with a small correction due to the ions), and stable Doppler-shifted electrostatic whistler waves. Both the beam modes and the whistlers are on separate branches of the linear dispersion relation. The frequency on the whistler branch is bounded below by $\max(\omega_i,\ kv_b\cos\theta)$ and the frequency on the beam-mode branch is bounded above by $\min(\omega_i,\ kv_b\cos\theta)$. The splitting into two branches is caused by the segregation of waves with $\omega > kv_b\cos\theta$ from those with $\omega < kv_b\cos\theta$. A new feature due to the presence of ions will be (weakly) unstable waves on the beam-mode branch near the lower-hybrid frequency.

4 Two-dimensional PIC simulation with dynamic ions

In this section, we review the results of recent particle-in-cell (PIC) simulations used to study the 2-D nonlinear evolution of the two-stream instability (Goldman et al., 1998, 1999; Oppenheim et al., 1999) These simulations include both dynamic hydrogen ions and a finite magnetic field ($\Omega_e/\omega_e = 5$). The simulation is initialized with two cold counterstreaming electron beams with equal densities $n_e/2$. A frame corresponding to the auroral ionosphere is chosen in which one of the beams has zero drift velocity and the other has velocity $\mathbf{v}_b = 5$ (in units of the *initial* thermal velocity of each electron component). The ions are put in the frame of the stationary electrons, with the same initial temperature.

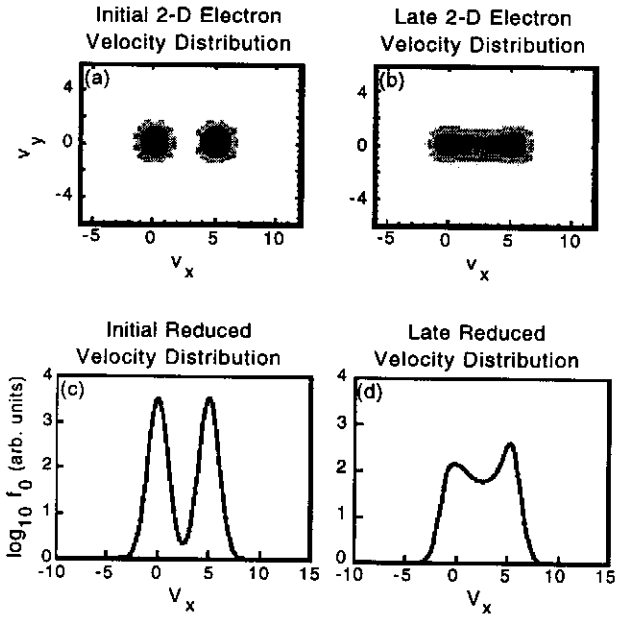

Fig. 6. Evolution of space-averaged electron velocity distribution in units of initial rms velocity-width of one of the beams.

4.1 Evolution of velocity distribution

As in 1-D simulations, the initial beams evolve after only a few plasma periods into a nonthermal electron velocity distribution elongated along **B**, as shown in Fig. 6. The reduced velocity distribution parallel to **B** evolves from two cold beams into a merged nonthermal distribution with residual velocity bumps. The total evolved distribution function has a drift velocity $v_d \approx v_b/2$ and a parallel rms (thermal velocity) $v_{\rm rms} \approx v_b/2$. The extreme elongation of the 2-D velocity distribution, the merged shape of the evolved distribution, and the ratio $v_d/v_{\rm rms} \sim O(1)$ are consistent with FAST measurements (Ergun et al., 1998). The asymmetry in the late-time reduced distribution is due to the presence of ions. Velocity distributions measured on FAST sometimes also appear to show residual velocity bumps.

4.2 Evolution of real-space electric fields

Snapshots of the real-space bipolar wave structures are shown in Figs. 7a and 7c. These are density plots of the normalized wave energy density $|\mathbf{E}(x,y)|^2$. The darker regions indicate higher energy densities. All distances are in units of the effective "Debye" length, $\lambda_e \equiv v_b/2\omega_e$. The bipolar wave structure in x (parallel to $\mathbf{v}_b$ and **B**) shows up as two peaks separated by a (zero-value) valley. Initially, there is no coherence in the y (transverse) direction. However, in Fig. 7a at time $\omega_e t = 640$, the structures have gained transverse coherence and are significantly wider in y than in x.

The horizontal structures are electrostatic whistler

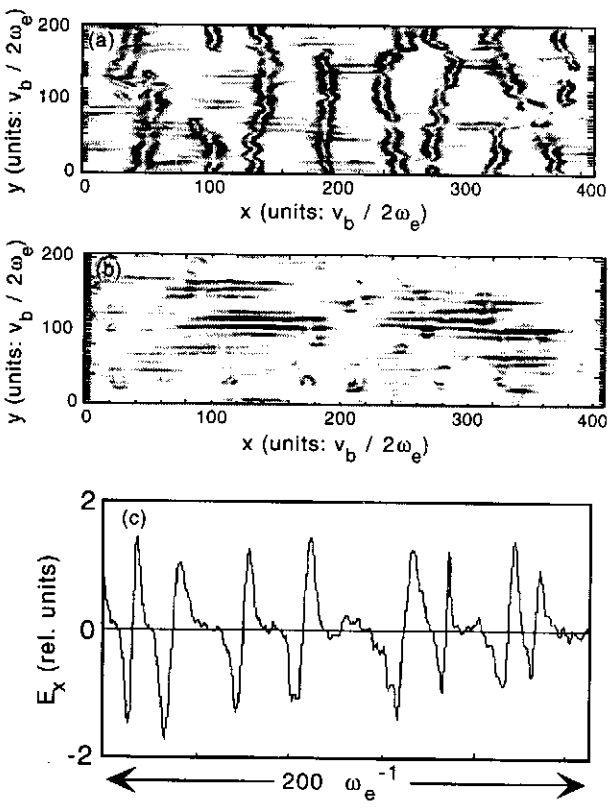

Fig. 7. Detail of $|\mathbf{E}(x,y)|^2$ at early time (a) showing bipolar structures and low-level whistlers, and at late whistler-dominated time (b). Frame (c) shows a time history of E_x at a fixed spatial point.

waves. These whistlers, unlike the bipolar structures, do not exhibit long-time spatial coherence. They propagate at several times the velocity of the bipolar structures in the $\pm x$ direction and both up and down along y. Figure 7b shows that at much later times ($\approx 1000\omega_e^{-1}$) the bipolar wave structures are less intense and exhibit a much smaller spatial half-width transverse to **B** (i.e., in the y direction). The whistlers dominate at late times when the bipolar structures are weaker and broken up transversely. At very late times, many of the remaining bipolar structures have comparable widths parallel and perpendicular to **B**, consistent with selected measurements (Ergun et al., 1998).

In Fig. 7c we have recorded $E_x(t)$ at a fixed point in the cell as the structures move by in order to simulate the spacecraft antenna wave measurements. The bipolar structure is evident. The inferred positive peak to negative peak spatial widths are typically $6\text{–}8\lambda_e$, in agreement with measured widths discussed above for the more intense events (Ergun et al., 1998). The maximum strength of the electric field is $E = 1.9(n_e T_e)^{1/2}$ V/m (for $n_e T_e$ in units of 100 eV cm^{-3}). This is higher than the fields analyzed in Ergun's data set (Ergun et al., 1998), but in reasonable agreement with other FAST

measurements of intense bipolar structures. (Carlson et al., 1998).

4.3 Wavenumber and frequency spectra

In Fig. 8 we present a different visualization of the results of the same 2-D simulation. Plots are furnished of the K_x–K_y and ω–$\mathbf{K}$ power-spectra, with $\mathbf{K} = \mathbf{k}v_b/2\omega_e$ and frequency in units of ω_e. In Fig. 8a the K_x–K_y power spectrum of the bipolar structures are confined in $\mathbf{K}$ space to a broad parallel range ΔK_x corresponding to their narrow spatial extent in x (no distinction is made between wave energy at $\pm K_x$), and to a narrow range ΔK_y centered about 0, corresponding to their broad coherence in the y direction. At earlier times, before the bipolar structures have gained coherence in the transverse direction, the K_x–K_y spectrum of the two-stream instability exhibits a much wider ΔK_y (Fig. 8b). The contour lines in Figs. 8a and 8b are the unstable mode growth rates obtained from the zeroes of (2). At the earlier time it is evident that the fastest growing modes correspond to the linear two-stream instability. The waves in Fig. 8a at very small angle to the perpendicular K_y axis are a mixture of electrostatic whistlers (W) and beam-modified lower hybrid (LH) waves.

Even more revealing is the ω–K_y power spectrum of Fig. 9 at fixed parallel wavenumber K_x =0.031. The peak power in the branches labeled "W" are about an order of magnitude greater than the peak power in the branch labeled "LH". The superimposed curves are the real (Doppler-shifted) frequencies found from the zeroes of (2). Note the surprisingly good fit to both the whistlers, which are stable according to linear theory, and to the unstable lower-hybrid branch. The peak intensity of the power spectrum is at $K \approx K_y = 0.3$, corresponding to $\theta \approx 84°$. At this angle, both ions and higher order electron terms can be neglected. The parallel group velocity of the whistlers is $v_x \approx (v_b/2)(1 \pm |K|^{-1}) \approx 4.3(v_b/2)$, so the whistler parallel velocity is much faster than the beam mode velocity, $v_b/2$, in agreement with the simulation.

We now turn to studies of the loss of coherence of the bipolar structures in the direction perpendicular to the magnetic field, and to the associated production of electrostatic whistler waves.

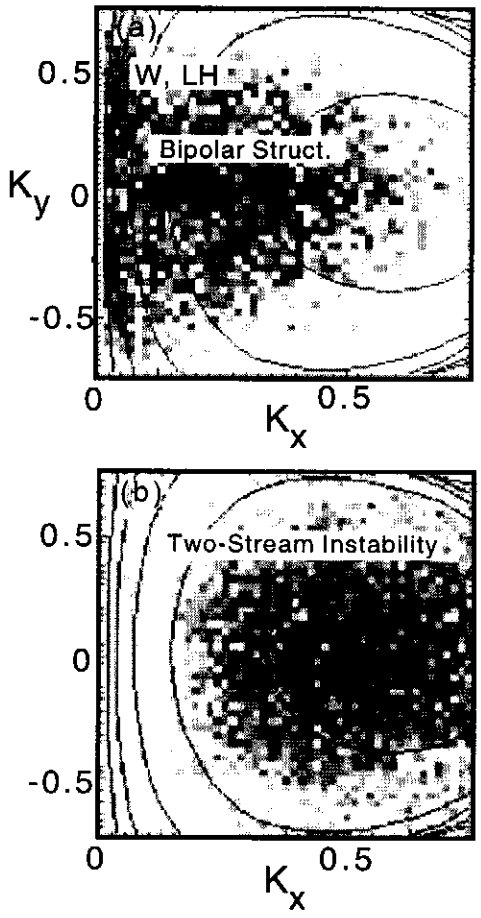

Fig. 8. Wave power spectra in K_x–K_y space at (a) late and (b) early time.

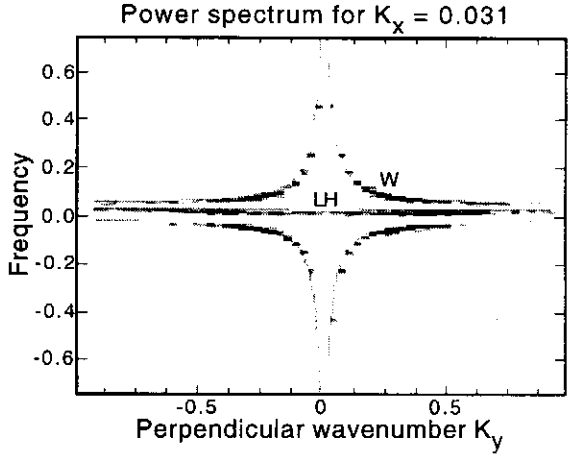

Fig. 9. Wave power spectrum in ω–K_y space at fixed value of K_x.

5 PIC simulations of breakup of idealized bipolar wave structures

In order to study the evolution of bipolar structures and electrostatic whistlers in two dimensions it is desirable to simplify the problem considerably. Simplification is possible at several levels.

First we note that, for the parameters considered, the evolution of bipolar structures and whistlers shown in Fig. 7 is virtually unchanged if the PIC code is run

with infinitely magnetized electrons, and qualitatively the same when a static homogeneous ion distribution is used. These simplifications enable simulations to be run longer and with greater resolution. The motion of electrons in the infinite magnetization limit is strictly one dimensional (along magnetic field lines), with the second dimension coming in only through Poisson's equation. The ions enter into Poisson's equation as a space and time independent neutralizing background density. Thus, the reduced Vlasov-Poisson system becomes

$$\left(\partial_t + v_x\partial_x + \frac{e}{m}\partial_x\phi\partial_v\right) f(x, v_x, y, t) = 0$$
$$\left[\partial_x^2 + \partial_y^2\right]\phi(x, y, t) = 4\pi e\left(\int_{-\infty}^{\infty} dv_x\, f - n_{i0}\right) \qquad (3)$$

To further simplify the simulations, we initiate the bipolar structures with an idealized form. This is accomplished (Oppenheim et al., 1999) by starting with a strictly one-dimensional PIC simulation of the two-stream instability and running it until a small number of well-separated phase-space holes (as in Fig. 3) remain. At that time, the 2-D PIC simulation is reinitialized with the x–v_x phase space structure from the 1-D startup extended uniformly into the (perpendicular) y direction. This creates straight *tubes* in the three-dimensional (x–v_x–y) phase space. These tubes correspond to the initially straight bipolar structures in $|\mathbf{E}(x, y)|^2$, as shown in Fig. 10a. The evolution of the bipolar structures in time is then apparent in Figs. 10b–10d. Figure 10e shows the evolution of a single bipolar structure as one rides along with it. It is clear that the straight tubes develop "ripples" simultaneously with the appearance and intensification of electrostatic whistlers (the horizontal wave structures in Fig. 10). The ripple frequency is approximately the same as the whistler frequency. Eventually the rippled bipolar structures tear apart, and the whistlers become very intense. This simplified evolution is consistent with the evolution of bipolar structures shown in Fig. 7 for the full 2-D run (with ions).

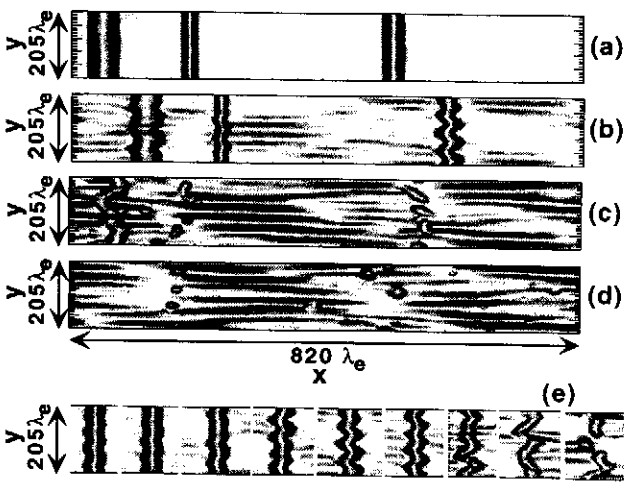

Fig. 10. $|\mathbf{E}(x, y)|^2$ from 2-D simulation initialized with straight phase-space tubes at (a) $t = 0$, (b) $t = 1716\omega_e^{-1}$, (c) $t = 2508\omega_e^{-1}$, and (d) $t = 3828\omega_e^{-1}$. Frame (e) contains a sequence of snapshots centered on a single (moving) bipolar field structure as it evolves.

6 Bipolar wave structures, BGK modes, and linear stability analysis

It may be possible to set up an analytic approach to model the breakup of bipolar structures and the emission of electrostatic whistlers. We seek to understand the behavior of linear perturbations to an initial straight tube in three dimensional x–v_x–y phase space. An idealized vortex tube can be modeled as a Bernstein Greene Kruskal or "BGK" mode (Bernstein et al., 1957) in x–v_x electron phase space—extended uniformly in the y direction. The strategy is to find an exact nonlinear solution to (3) for f and ϕ which is independent of y and t. There are an infinite number of such solutions, so the challenge is to find a solution relevant to the bipolar structures in the simulations. A general BGK solution in 1-D (with static ions) consists of a stationary distribution of electrons $f_0(x, v_x)$ and a potential $\phi_0(x)$. We assume $\phi_0(x)$ to be unimodal and symmetric about $x = 0$. It is easy to show that f_0 must be a function of constants of the motion of the characteristic trajectories for the Vlasov-Poisson equations. One such constant is the energy

$$w = \frac{m}{2}v^2 - e\phi_0(x) \qquad (4)$$

For a potential energy trough of the kind in Fig. 4, there are three classes of electrons and corresponding distribution functions for each: trapped electrons, untrapped or "passing" electrons with positive velocity, and passing electrons with negative velocity. For the passing electrons, the sign of the velocity is a constant of the motion. The trapped electrons correspond to negative energies in the range $\phi_0(0) < w < 0$, while for the passing electrons $w > 0$. The orbits in phase space are shown in Fig. 11. The trapped and untrapped orbits are separated by a *separatrix* orbit defined by $w = 0$. The BGK solutions we seek here should not only have a potential with a shape as in Fig. 4, but the distribution function should go to zero at large positive energies and vanish for a range of negative energies near the bottom of the potential well in order to have a phase space hole that resembles the one shown in Fig. 3. A reasonable additional assumption is that the passing electron distribution functions be identical for positive and negative velocities.

Even with these constraints, many solutions can be constructed. There are three components to a 1-D stationary BGK solution to (3): the potential $\phi_0(x)$, the trapped electron distribution $f_T(w)$, and the untrapped

(passing) electron distribution function $f_U(w)$. Any two of these components may be chosen arbitrarily and the third found by using Poisson's equation—although the third component so determined may not be physical. Typically, the potential is taken to be a gaussian with $\phi_0 = \phi_{\max} \exp(-x^2/2a^2)$ (Muschietti et al., 1998; Turikov, 1984; Krasovsky et al., 1997), or a hyperbolic function, such as $\phi_0 = \phi_{\max} \operatorname{sech}^4(x/2a)$ (Schamel, 1982; Turikov, 1984). Then, for example, one may assume a relatively simple form for f_U and solve for f_T. Such a procedure was carried out for the FAST data set, using a gaussian potential by Muschietti et al. (1998).

In order to interpret the breakup of bipolar structures and the growth of electrostatic whistlers as a possible instability of a BGK "state" $\{f_0(w),\ \phi_0(x)\}$, one can linearize (3) about the spatially nonuniform BGK state. That is, we seek the properties of perturbations, f_1 and ϕ_1 in the expansions $f = f_0(w) + f_1(x, y, v_x, t) + \ldots$ and $\phi = \phi_0(x) + \phi_1(x, y, t) + \ldots$ The linear problem is an eigenvalue problem which is often very challenging to solve. Few studies of the stability of BGK solutions exist (Schamel, 1982; Goldman, 1970). In this paper, we simply set up the full problem. The linearized Vlasov equation (3) is formally solved in terms of the first-order potential ϕ_1 by a Green's function (Goldman, 1970) and inserted into Poisson's equation for ϕ_1 to yield

$$\begin{aligned}(-\partial_x^2 \ + \ k_y^2)\phi_1(x,t) &= 4\pi\rho_1(x,t) \\ &= -c\int_0^t dt'\,dx'\,dv'\,\delta[x - x_{\rm orb}(t-t';x',v')]\times \\ &\quad \times\{\partial_{v'} f_0(x',v')\}\partial_{x'}\phi_1(x',v') \qquad (5)\end{aligned}$$

with the orbits satisfying

$$\begin{aligned}\partial_t x_{\rm orb} &= v_{\rm orb}(t-t';x',v'), & x_{\rm orb}(0) &= x' \\ \partial_t v_{\rm orb} &= \frac{e}{m}\partial_{x_{\rm orb}}\phi_0(x_{\rm orb}), & v_{\rm orb}(0) &= v' \qquad (6)\end{aligned}$$

The source term $\partial_{v'} f_0 \partial_{x'}\phi_1$ in (5) acts at the phase space point $\{x', v'\}$ at time t', and the delta-function guarantees that this information propagates to the point $\{x, v\}$ at the later time t along the orbits $\{x_{\rm orb},\ v_{\rm orb}\}$ given by (6) and illustrated in Fig. 11. The constant c is just $4\pi e^2/m$. The k_y term arises because we have Fourier transformed in y. If we Fourier transform in time, thereby introducing ω, and replace the velocity v' by the energy w defined in (4), a differential-integral equation is obtained which must be solved together with eigenvalues k_y or ω.

7 Conclusions

Using numerical simulations and heuristic arguments, the nonlinear two-dimensional evolution of a classic two-stream instability has been shown to lead to bipolar

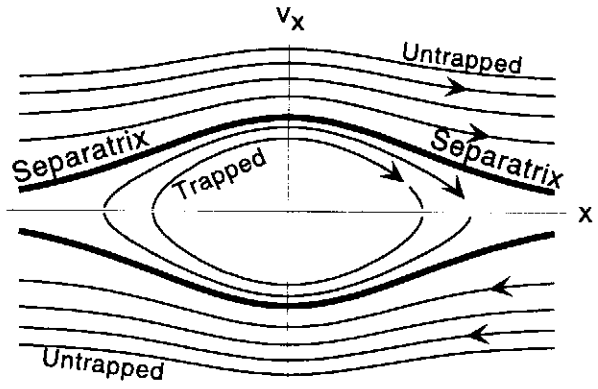

Fig. 11. Trapped and untrapped orbits separated by a *separatrix* in the electrostatic potential associated with bipolar field structures.

wave structures exhibiting a number of the properties measured on board the FAST satellite in the auroral ionosphere. The simulations show that after thousands of plasma periods these structures lose their coherence across magnetic field lines and break up into weaker bipolar wave structures with an aspect ratio closer to one. The breakup process is accompanied by the emission of electrostatic whistlers which eventually come to dominate the bipolar structures.

A formal method has been set up for studying the linear stability of idealized stationary two-dimensional bipolar structures modeled as BGK solutions to the Vlasov-Poisson equations in the limit of strongly magnetized electrons and static ions.

There are several possible routes to an explanation of the instability of idealized bipolar structures such as those observed in the simulation of Fig. 10. The first-order density of whistlers moving through the bipolar structures may destabilize the trapped particle equilibrium. To show this would require a kinetic approach, based on a solution of (5). We have made some progress in this direction and results will be presented elsewhere.

It is also possible that the destabilization of coherent bipolar wave structures involves more than one such structure. The long parallel wavelength of the whistlers enables them to interact with more than one bipolar structure and to "come around again" to the same structure in a simulation with periodic boundary conditions. Preliminary numerical simulations based on a Vlasov code suggest that the straight bipolar structures may have their own low-frequency "normal mode," which can resonate with a whistler, leading to growth of the whistler.

Acknowledgements. We wish to thank Frank Crary, Fernando Perez, and Michael Spector for valuable discussions. This research was supported by grants from NASA (NAG5-4099), the National Science Foundation (ATM-9417116 and ATM-9802209), and the Department of Energy (DE-FG03-98ER54502). The numerical simulations were performed at the Advanced Computing Laboratory of Los Alamos National Laboratory.

References

Berk, H. L. and Roberts, K. V. Nonlinear study of Vlasov's equation for a special class of distribution functions. *Phys. Fl., 10*, 1595–1610, 1967

Bernstein, I. B., Greene, J. M., and Kruskal, M. D., Exact nonlinear plasma oscillations. *Phys. Rev. Lett., 108*, 546–550, 1957

Carlson, C. W., *et al.*, FAST observations in the downward auroral current region: Energetic upgoing electron beams, parallel potential drops and ion heating., *Geophys. Res. Lett., 25*, 2017–2020, 1998

Ergun, R. E., Carlson, C. W. McFadden, J. P., Mozer, F. S., Muschietti, L., Roth, I., and Strangeway, R., Debye-scale plasma structures associated with magnetic-field-aligned electric fields. *Phys. Rev. Lett., 81*, 826–829, 1998

Goldman, M. V., Theory of stability of large periodic plasma waves, *Phys. Fluids, 13*, 1281–1289, 1970

Goldman, M. V., Oppenheim, M. M., and Newman, D. L., PIC Simulations of bipolar wave structures driven by dense beams in the auroral ionosphere, in *Physics of Space Plasmas, 15*, edited by T. Chang and J. R. Jasperse, pp. 115–120, MIT Center for Theoretical Geo/Cosmo Plasma Physics, Cambridge, MA, 1998.

Goldman, M. V., Oppenheim, M. M., and Newman, D. L., Nonlinear two-stream instabilities as an explanation for auroral bipolar wave structures. *Geophys. Res. Lett.*, in press, 1999

Krasovsky, V. L., Matsumoto, H., and Omura, Y., Bernstein-Greene-Kruskal analysis of electrostatic solitary waves observed with Geotail. *J. Geophys. Res., 102*, 22,131–22,139, 1997

Morse, R. L., and Nielson, C. W., One, two and three-dimensional simulation of two-beam plasmas. *Phys. Rev. Lett., 23*, 1087–1090, 1969

Muschietti, L.,Ergun, R. E., Roth, I., and Carlson, C. W., Phase-space electron holes along magnetic field lines. *Geophys. Res. Lett., 26*, 1093–1096, 1999

Omura, Y., Matsumoto, H., Miyake, T., and Kojima, H., Electron beam instabilities as generation mechanism of electrostatic solitary waves in the magnetotail. *J. Geophys. Res., 101*. 2685 2697, 1996

Oppenheim, M. M., Newman, D. L., and Goldman, M. V., Evolution of electron phase-space holes in a 2-D magnetized plasma. *Phys. Rev. Lett.*, submitted, 1999

Schamel, H., Stability of electron vortex structures in phase space, *Phys. Rev. Lett., 48*, 481–483, 1982

Turikov, V. A., Electron phase space holes as localized BGK solutions. *Phys. Scr. 30*, 73, 1984